Supplemental Methods

Immunohistochemistry and quantification For hypoxia analysis, mice were injected with 60 mg/kg of pimonidazole 1 h before tumor removal. Tumor tissue samples were harvested and fixed for 2 hours in 4% formaldehyde. After fixation, tissue was incubated in 30% sucrose solution overnight at 4°C. Then, samples were embedded in OCT compound (Tissue-Tek) and kept at -80°C. Frozen blocks were cut at 20 μm thickness, and stained for CD31 (1:100, BD Biosciences, catalog# 550274) or fractalkine (CX_3CL1) (1:100, Abcam, catalog# ab25088), and counterstained with DAPI (Vector Labs) according to the manufacture's protocol. Whole tumor tissue images were taken using an Olympus FV1000 confocal laser-scanning microscope. Fractalkine positive area and hypoxic area were quantified using custom codes in MATLAB (The MathWorks). For vascular analysis, vessels were skeletonized and segmented using a custom, semi-automated tracing program developed in MATLAB (The MathWorks), allowing the removal of structures under 30 pixels and regions of autofluorescence.

Clinical specimens immunohistochemistry We obtained biopsies of rectal carcinomas from patients before and 12 days after bevacizumab treatment (1, 2). Formalin-fixed paraffin-embedded rectal carcinoma biopsy samples were cut at 5-μm thickness. The sections were stained with anti-fractalkine (CX_3CL1) antibody (R&D Systems, catalog# AF365) according to the manufacture's protocol. Fractalkine positive area was quantified using custom codes in MATLAB (The MathWorks).

Flow cytometry Flow cytometry was performed as described previously (3). Briefly, tumor tissues were resected, chopped, and digested in a 37°C incubator for 1 hour with culture medium containing collagenase type 1A (1.5 mg/mL), hyaluronidase (1.5 mg/mL), and DNase (2 mg/ml). Digested tissue was filtered through 70-μm cell strainers. The single cell suspensions were incubated with a rat anti-mouse CD16/CD32 antibody (BD Bioscience, clone# 2.4G2) and then were stained with the following monoclonal antibodies according to the manufacturer's protocols: CD45 (BD Bioscience, clone# 30-F11), B220 (clone# RA3-6B2), CD49b (clone# DX5), CD90 (clone# 53-2.1), Ter119 (clone# TER-119), I-A/I-E (clone# M5/114.15.2), NK1.1 (clone# PK136), CD4 (clone# RM4-5), CD8 (clone# 53-

6.7), Granzyme B (clone# NGZB), PD-1 (clone# J43), FoxP3 (clone# FJK-16s), CD25 (clone# PC61), CD11b (clone# M1/70), F4/80 (clone# BM8), CD11c (clone# HL3), Gr1 (clone# RB6-8C5), Ly6C (clone# HK1.4), Ly6G (clone# 1A8) (BD Biosciences). 7-Amino-actinomycin D (7AAD) reagent (eBioscience, clone# 00-6993-50) was added to the stained tubes just before running the flow cytometer. We defined $CD45^+$ Lin^- $F4/80^-$ $CD11c^-$ $CD11b^+$ $Ly6G^-$ ($Ly6C^{low}$ or $Ly6C^{high}$) population as $Ly6C^{low}$ or $Ly6C^{high}$ monocytes. We defined $CD45^+$ Lin^- $F4/80^-$ $CD11c^-$ $CD11b^+$ $Ly6G^+$ population as neutrophils. After staining, flow cytometry was performed using an LSRII flow cytometer (Becton Dickinson, Franklin Lakes, NJ), and the data were analyzed with FlowJo software (Tree Star, Ashland, OR).

Gene expression polymerase chain reaction (PCR) array Total RNA was extracted from each sorted subset of myeloid cells by RNeasy Mini Kit (QIAGEN, Venlo, Netherlands). Relative gene expression was determined using RT^2 *Profiler* PCR Arrays system (QIAGEN, Venlo, Netherlands) on a Mx3000P qPCR System (Stratagene, La Jolla, CA). The pre-made pathway-focused arrays used (mouse genes) were “Chemokines & Receptors (PAMM022Z)” and “T-Cell & B-Cell Activation (PAMM053Z)”.

Quantitative reverse-transcription PCR Total RNA was extracted from resected tumor tissues by RNeasy Mini Kit (QIAGEN, Venlo, Netherlands). cDNA products were synthesized by iScript reverse transcription supermix (Bio-Rad Laboratories, Hercules, CA). Relative gene expressions of *Bv8* (forward primer: GCCCCGCTACTGCTACTTC; reverse primer: CCCCGTGCAGACACTAACTTT), *Tie2* (forward primer: GAGTCAGCTTGCTCCTTTATGG; reverse primer: AGACACAAGAGGTAGGGAATTGA), and *Cx3cl1* (forward primer: CGCGTTCTTCCATTTGTGTA; reverse primer: CTGTGTCGTCTCCAGGACAA) were determined using the specific primers, Real-Time SYBR Green PCR master mix (Applied Biosystems, Branchburg, NJ), and a Mx3000P qPCR System (Stratagene, La Jolla, CA). All values were normalized by GAPDH as a reference gene.

Western blot analysis Serum-starved mouse primary lung microvascular endothelial cells (LMVECs) were treated with control buffer or recombinant VEGF-A protein (50 ng/ml) in the absence or presence of 2 μg/ml DC101 for 12 hrs. After treatment, the cells were lysed with RIPA buffer (Thermo Scientific) with protease and phosphatase inhibitors. Total protein concentration was determined by the Pierce BCA protein assay kit (Thermo Scientific). Each lane was loaded with equal amounts of total protein. Blots were probed with goat anti-mouse CX3CL1 antibody (R&D Systems, catalog# AF472) and donkey anti-goat IgG-HRP (Santa Cruz Biotechnology, catalog# sc-2020) antibody, and developed with Amersham ECL Prime Western blotting detection reagents (GE-Healthcare Life Sciences). Each tumor sample was homogenized directly in lysis buffer for protein extraction. 30 μg of denatured protein per sample was loaded on 10% SDS-polyacrylamide gels. Membranes were blotted with antibodies against CX3CL1 (R&D Systems, catalog# AF472) and GAPDH (Cell Signaling, catalog# 2118). Antibodies were diluted 1:1000.

Protein expression measurement For multiplex array, each tumor sample was homogenized directly in lysis buffer for protein extraction. 2 μg/μl of sample was used for the pre-made inflammatory multiple cytokines protein array (V-PLEX Proinflammatory Panel 1 mouse kit, Cat. # K15048D). To measure other cytokine/chemokine expression levels, we used mouse Quantikine ELISA kits for TGF-β1, CXCL2, CXCL5, CX3CL1, and CCL2 (R&D systems) following the manufacturer's protocols. $Ly6C^{low}$ monocytes, $Ly6C^{high}$ monocytes, and neutrophils were sorted (FACS Aria) from SL4 tumor-bearing C57BL/6 mice treated with DC101. The sorted cells were cultured for 24 h, and their conditioned media were collected for cytokine/chemokine level measurement according to the manufacturer's protocols.

***In vitro* migration assay** $Ly6C^{low}$ monocytes, $Ly6C^{high}$ monocytes, and neutrophils were sorted (FACS Aria) from SL4 tumor-bearing C57BL/6 mice treated with DC101. 2 X 10^4 neutrophils were seeded on 3 μm pore size PET membrane transwell inserts (Corning) in the upper chamber. The lower

chamber included either 8 X 10^4 Ly6C^{low} monocytes, Ly6C^{high} monocytes, or their conditioned media with or without neutralizing antibodies for the chemokine/chemokine receptor. Anti-CXCR2 antibody (10 μg/ml) (R&D systems, catalog# MAB2164-100), anti-CXCL1 antibody (2 μg/ml) (R&D systems, catalog# MAB453-SP), anti-CXCL2 antibody (2 μg/ml) (R&D systems, catalog# MAB452-SP), and anti-CXCL5 antibody (2 μg/ml) (R&D systems, catalog# MAB433-SP) were used. After 5 h, non-migrated cells were removed with a cotton tip and the membranes were fixed and stained with Protocol HEMA 3 staining solutions (Fisher Scientific) to identify cells that had migrated to the lower surface of the membrane. The number of migrated cells was determined using 200X magnification.

CFSE T cell proliferation assay CD8$^+$ T cells and CD4$^+$ T cells were sorted (FACS Aria) from spleens of C57BL/6 wild-type mice. The sorted CD8$^+$ and CD4$^+$ T cells were incubated with CellTrace CFSE (5 μM) at 37°C for 15 min and washed with pre-warmed RPMI-1640 media with 5% FBS. CFSE-labeled CD8$^+$ or CD4$^+$ T cells (2 X 10^4 cells) were co-cultured with Ly6C^{low} monocytes, Ly6C^{high} monocytes, or neutrophils (1:2 ratio) for 2 days with or without anti-IL-10 neutralizing antibody (10 μg/ml, BD, Clone JES5-2A5) in the presence of anti-CD28 antibody (2 μg/ml, Abcam, clone 37.51) in a 96 well plate pre-coated with anti-CD3e antibody (Abcam, clone 145-2C11). Ly6C^{low} monocytes, Ly6C^{high} monocytes, and neutrophils were sorted (FACS Aria) from SL4 tumor-bearing C57BL/6 mice treated with DC101. CFSE levels were assessed in CD8$^+$ and CD4$^+$ T cells by flow cytometry using an LSRII flow cytometer.

Adoptive transfer For the rescue effect of adoptive transfer, Ly6C^{low} monocytes and Ly6C^{high} monocytes were sorted (FACS Aria) from SL4 tumor-bearing C57BL/6 wild-type or *Cx$_3$cr1$^{-/-}$* mice treated with DC101. 1 X 10^6 of sorted Ly6C^{low} monocytes (i.e., WT Ly6C^{low} monocytes or CX3CR1-deficient Ly6C^{low} monocytes) or WT Ly6C^{high} monocytes were intravenously injected twice a week into *Cx$_3$cr1$^{-/-}$* mice treated with DC101 from the beginning of DC101 treatment. For intravital microscopy, Ly6C^{low} monocytes were sorted (FACS Aria) from SL4 tumor-bearing C57BL/6 wild-type or *Cx$_3$cr1$^{-/-}$* mice treated with DC101. 1 X 10^6 of sorted wild-type Ly6C^{low} monocytes (WT Ly6C^{low} monocytes) and

CX3CR1-deficient Ly6C^{low} monocytes (KO Ly6C^{low} monocytes) were fluorescently labeled with Vybrant DiO cell-labeling solution (Thermo Scientific) according to the manufacturer's protocol, and then intravenously injected into C57BL/6 wild-type mice treated with DC101.

Cecum window Eight to ten-week-old male mice were anesthetized with intraperitoneal injection of ketamine (100 mg/kg) and xylazine (10 mg/kg). Abdominal hair was removed, and 10 mm mid-line incision was made to expose the cecum. A glass coverslip was put in a metal ring and fixed with a coverslip holder, and the metal ring was glued to the cecum. Using a purse-string suture (Ethicon, Somerville, NJ), the abdominal wall and skin were placed in the side groove of the metal ring, and the purse-string suture loop was tightened.

Optical system and *in vivo* CRC imaging The imaging platform was a previously described custom-built video-rate multi-photon fluorescence microscope (4). The system acquired three-color images (512 x 512 pixels) at 30 frames per second. The images are displayed in real time on a computer monitor and streamed to a hard disk. The custom data acquisition program can also display and record images averaged over an arbitrary number of consecutive frames in real time. A three-axis translation stage was used to move the mouse. To visualize the blood vessels, 100 μl of tetramethylrhodamine-isothiocyanate (TRITC)-Dextran (5 mg/ml) was injected intravenously.

Cell counting and cellular perfusion rate *in vivo* To determine the number of CX_3CR1^+ cells and adoptively transferred Ly6C^{low} monocytes, images were acquired at arbitrarily chosen sites with a FOV of 512 μm each. The image acquisition took approximately 1 minute at each site. The average number of cells was counted and divided by the image area (i.e., 512 μm x 512 μm) to calculate the cell density per 1 mm^2 in area of tissue. The number of flowing (at a speed of >0.2 mm/s), rolling (15-50 μm/s) and crawling (<15 μm/s) cells in the blood vessels was counted from the acquired video-rate movies. The cellular perfusion rate, or flux, was defined as the total number of moving cells per unit area per unit time (i.e., divided by the recording time period).

Synthesis and *in vitro* screening of siRNA Twelve siRNAs with the lowest predicted off-target potentials and 100% homology with mouse CX3CL1 gene sequence NM_009142.3 were selected for synthesis and screening. Single-strand RNAs were produced and annealed at Axolabs GmbH and used as duplexes. Mouse primary lung microvascular endothelial cells (LMVECs) were transfected with siRNA by using Lipofectamine 2000 reagent (Thermo Scientific) according to the manufacturer's protocol at 0.1 nM and 10 nM concentrations. CX3CL1 mRNA levels were quantified 24 hours after transfection by quantitative RT-PCR and normalized to GAPDH mRNA. Duplexes showing best knockdown at both concentrations (indicated by red box in Figure 7B) were selected for 6-point dose-response ranging from 6 pM up to 20 nM. The best duplex with the sequence 5'-gcuuGcGAGAGGGuuuAAAdTsdT-3' (sense) and 5'- UUuAAACCCUCUCGcAAGCdTsdT-3' (anti-sense) was selected for large-scale synthesis, nanoparticle formulation, and subsequent *in vivo* work. Lower case represents 2'-O-methyl modification. These modifications protect siRNA from endonucleolytic degradation and repress potential immune-stimulatory properties of the siRNA, which are crucial for *in vivo* applications. The sulfur modification in dTsdT residue protects the oligonucleotide from 3'-5'-exonucleolytic degradation. Also, siRNA against CX3CL1 from a recent publication (Morari et al., 2014) was used for the knockdown efficiency comparison with the following sequence: 5'-GCCGCGUUCUUCCAUU-3' (sense) and 5'-ACAAAUGGAAGAACGC-3' (anti-sense). For silencing Tie2 (siTIE2), we used a duplex with the following sequence: 5'-GAAGAuGcAGuGAuuuAcAdTsdT-3' (sense) and 5'-UGuAAAUcACUGcAUCUUCdTsdT-3' (anti-sense). For the control siRNA against Luciferase (siLUC), we used a duplex with the following sequence: 5'-cuuAcGcuGAGuAcuucGAdTsdT-3' (sense) and 5'- UCGAAGuACUcAGCGuAAGdTsdT-3' (anti-sense).

siRNA formulation into 7C1 nanoparticles Purified 7C1 nanoparticles were synthesized and formulated as previously described (5). Specifically, polyethyleneimine with a number molecular weight of 600 (PEI_{600}, Sigma Aldrich) was combined with 200 proof anhydrous ethanol (Koptec) and an epoxide-terminated C_{15} lipid at a lipid:PEI molar ratio equal to 14:1. The mixture was heated at 90˚C for

48 hours before purification was performed with a silica column as previously described (5). To formulate nanoparticles, purified 7C1 was combined with 200 proof ethanol and (1,2-dimyristoyl-sn-glycero-3-phosphoethanolamine-N-[methoxy(polyethylene glycol)-2000] (Avanti Polar Lipids) at a 7C1:lipid-PEG molar ratio equal to 4:1 in a glass syringe. siRNA was dissolved in pH 3 10 mM citrate solution (Teknova) in a separate syringe. The two syringes were connected to a syringe pump and the fluid was pushed through a microfluidic device as previously described (6). The resulting nanoparticles were dialyzed in 1x PBS and sterilized using a 0.22 μm poly(ether sulfone) syringe filter (Genesee Scientific).

Nanoparticle characterization Nanoparticle size and structure was analyzed by dynamic light scattering (DLS) (Zetasizer NanoZS, Malvern Instruments)or cryogenic transmission electron microscopy (cryo-TEM) as previously described (5). DLS samples were measured in sterile 1X PBS at an approximate siRNA concentration of 1.0-3.0 μg/mL. Cryo-transmission electron microscopy (TEM) samples were prepared in a controlled environment vitrification system at 25 °C and ~ 100% relative humidity.

Supplemental References

1. Willett CG, Duda DG, di Tomaso E, Boucher Y, Ancukiewicz M, Sahani DV, Lahdenranta J, Chung DC, Fischman AJ, Lauwers GY, et al. Efficacy, safety, and biomarkers of neoadjuvant bevacizumab, radiation therapy, and fluorouracil in rectal cancer: a multidisciplinary phase II study. *Journal of clinical oncology : official journal of the American Society of Clinical Oncology.* 2009;27(18):3020-6.
2. Xu L, Duda DG, di Tomaso E, Ancukiewicz M, Chung DC, Lauwers GY, Samuel R, Shellito P, Czito BG, Lin PC, et al. Direct evidence that bevacizumab, an anti-VEGF antibody, up-regulates SDF1alpha, CXCR4, CXCL6, and neuropilin 1 in tumors from patients with rectal cancer. *Cancer research.* 2009;69(20):7905-10.
3. Huang Y, Yuan J, Righi E, Kamoun WS, Ancukiewicz M, Nezivar J, Santosuosso M, Martin JD, Martin MR, Vianello F, et al. Vascular normalizing doses of antiangiogenic treatment reprogram the immunosuppressive tumor microenvironment and enhance immunotherapy. *Proceedings of the National Academy of Sciences of the United States of America.* 2012;109(43):17561-6.
4. Kirkpatrick ND, Chung E, Cook DC, Han X, Gruionu G, Liao S, Munn LL, Padera TP, Fukumura D, and Jain RK. Video-rate resonant scanning multiphoton microscopy: An emerging technique for intravital imaging of the tumor microenvironment. *Intravital.* 2012;1(1).
5. Dahlman JE, Barnes C, Khan OF, Thiriot A, Jhunjunwala S, Shaw TE, Xing Y, Sager HB, Sahay G, Speciner L, et al. In vivo endothelial siRNA delivery using polymeric nanoparticles with low molecular weight. *Nat Nanotechnol.* 2014;9(8):648-55.
6. Chen D, Love KT, Chen Y, Eltoukhy AA, Kastrup C, Sahay G, Jeon A, Dong Y, Whitehead KA, and Anderson DG. Rapid discovery of potent siRNA-containing lipid nanoparticles enabled by controlled microfluidic formulation. *J Am Chem Soc.* 2012;134(16):6948-51.

Supplemental Figures

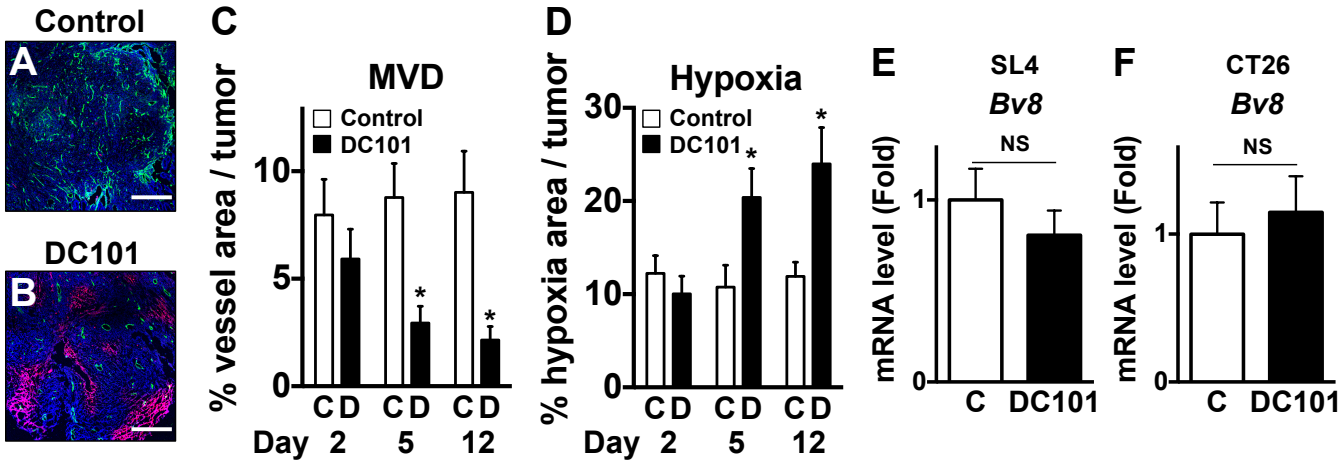

Figure S1. Anti-VEGFR2 therapy induces vessel regression and hypoxia in CRCs. (**A-B**) Representative images showing $CD31^+$ blood vessels (green) and hypoxia (red) in SL4 tumors grown orthotopically in C57BL/6 WT mice treated with either control rat IgG (A) or DC101 (B) analyzed on day 12. Blue, DAPI. Scale bar, 300 μm. (**C**) $CD31^+$ area percentage of total viable area (microvessel density) from SL4 tumors of control (C) and DC101 (D) groups. Data are represented as mean ± SEM. n=5/group. Two-tailed t test. *, $p < 0.05$ versus control. (**D**) Hypoxic area percentage of total viable area (hypoxia) from SL4 tumors of control (C) and DC101 (D) groups. Data are represented as mean ± SEM. n=5/group. Two-tailed t test. *, $p < 0.05$ versus control. (**E** and **F**) Relative gene expression levels of Bv8 in SL4 (E) and CT26 tumors (F) were determined by quantitative real-time PCR, normalized against GAPDH. C57BL/6 and BALB/c WT mice bearing orthotopically grown syngeneic CRCs were treated with either control rat IgG (C) or DC101, and mRNA levels were analyzed on day 12. Data are represented as mean ± SEM. n = 5 / group. Two-tailed t test. NS, non-significant.

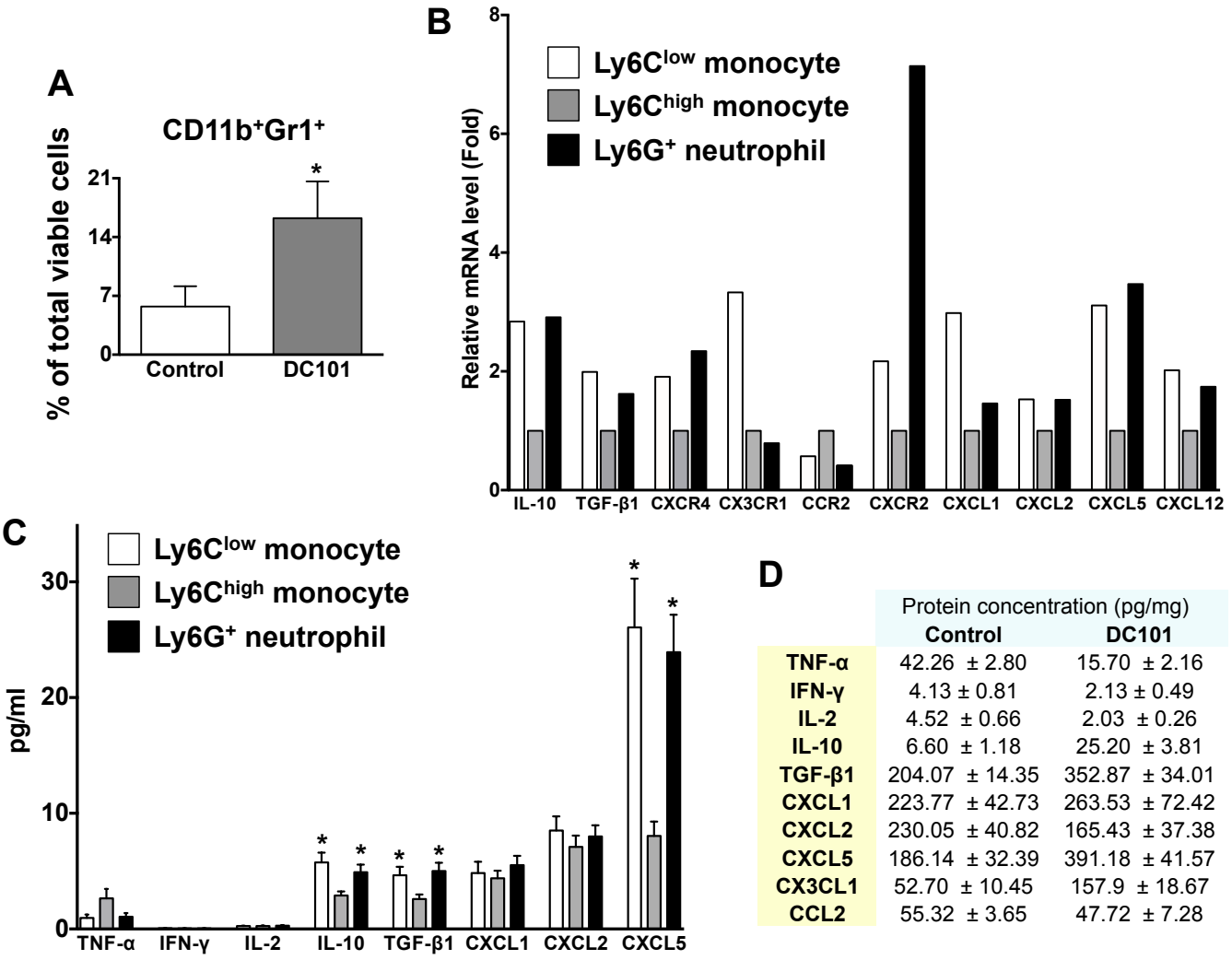

	Protein concentration (pg/mg)	
	Control	**DC101**
TNF-α	42.26 ± 2.80	15.70 ± 2.16
IFN-γ	4.13 ± 0.81	2.13 ± 0.49
IL-2	4.52 ± 0.66	2.03 ± 0.26
IL-10	6.60 ± 1.18	25.20 ± 3.81
TGF-β1	204.07 ± 14.35	352.87 ± 34.01
CXCL1	223.77 ± 42.73	263.53 ± 72.42
CXCL2	230.05 ± 40.82	165.43 ± 37.38
CXCL5	186.14 ± 32.39	391.18 ± 41.57
CX3CL1	52.70 ± 10.45	157.9 ± 18.67
CCL2	55.32 ± 3.65	47.72 ± 7.28

Figure S2. Identification of three distinct subsets of innate immune cells in CRCs. (**A**) $CD11b^{+}Gr1^{+}$ cells in SL4 tumors. C57BL/6 WT mice bearing SL4 tumors were treated with either control rat IgG or DC101. $CD11b^{+}Gr1^{+}$ cells in tumor infiltrate were analyzed on day 12 by flow cytometry. Data are represented as mean ± SEM. n = 8 / group. Two-tailed t tests. *, $p < 0.05$ versus control. Data are representative of three independent experiments. The graph depicts data for $CD11b^{+}Gr1^{+}$ population relative to total viable cells. (**B**) Relative gene expression level of tumor-isolated each subset of myeloid cells compared to $Ly6C^{high}$ monocytes. 4 samples were pooled into a PCR array plate. (**C**) Protein levels measured from conditioned media from culture of tumor-isolated each subset of myeloid cells. Data are represented as mean ± SEM. n = 5 / group. ANOVA with Holm-Sidak post-hoc test. *, $p < 0.05$ versus $Ly6C^{high}$ monocytes. The expression level of immunosuppressive cytokines (IL-10 and TGF-β1) are high in both $Ly6C^{low}$ monocytes and $Ly6G^{+}$ neutrophils, and relatively

low in Ly6C^{high} monocytes. Ly6C^{high} monocytes do not seem to play an important role in immunosuppression in this model shown by their low number and less-immunosuppressive phenotype. A chemokine known to attract CXCR2^{+} granulocytic cells (e.g., Ly6G^{+} neutrophils) is upregulated in Ly6C^{low} monocytes and neutrophils (i.e., CXCL5). (**D**) C57BL/6 WT mice bearing syngeneic orthotopic SL4 tumors were treated with either control rat IgG or DC101. Protein levels were measured from tumor tissue lysates. Relative protein expression level of DC101-treated tumors compared to control tumors is shown in **Figure 6A**. Data are represented as mean ± SEM. n = 5 / group.

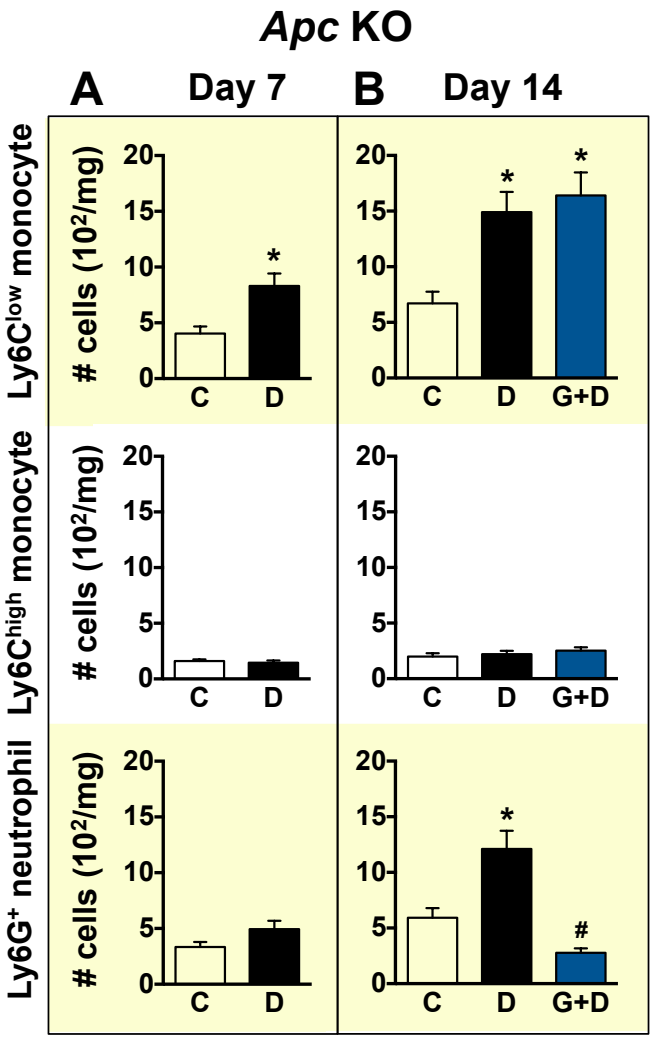

Figure S3. Anti-VEGFR2 therapy facilitates early infiltration of Ly6C^{low} monocytes into spontaneous rectal tumors. (**A** and **B**) Monocytes and neutrophils in spontaneous rectal tumors. Conditional *Apc* knock-out mice bearing spontaneous rectal tumors were treated with either control rat IgG (C), DC101 (D), or anti-Ly6G antibody + DC101 (G+D). Each subset of myeloid cells in tumor infiltrate was analyzed on day 7 (**A**) and 14 (**B**) by flow cytometry. *Top row*, Ly6C^{low} monocyte; *center row*, Ly6C^{high} monocyte; *bottom row*, Ly6G^{+} neutrophil. Data are represented as mean ± SEM. n = 7 / group. *, $p < 0.05$ versus control. #, $p < 0.05$ versus DC101. The graphs depict data for the absolute number of cells per mg of tumor tissue.

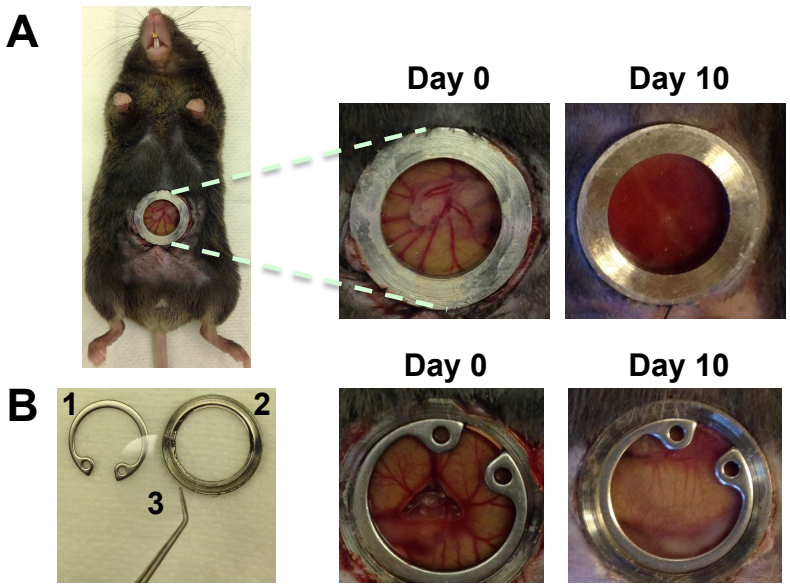

Figure S4. Development of the cecum window. (**A**) The initial version of the cecum window on a live mouse. At day 10 after implementation of the cecum window, body fluid (i.e., exudate) is accumulated. (**B**) Modified version of the cecum window on a live mouse. Components of the cecum window are shown; coverslip holder (1), metal ring (2), glass coverslip (3). At day 10 after implementation of the cecum window, body fluid (i.e., exudate) is cleared away by removing the old coverslip and replacing it with a new coverslip. Our unique cecum window developed for this study allows longitudinal imaging for over 4 weeks, unparalleled by other imaging windows applicable only for acute or short-term monitoring.

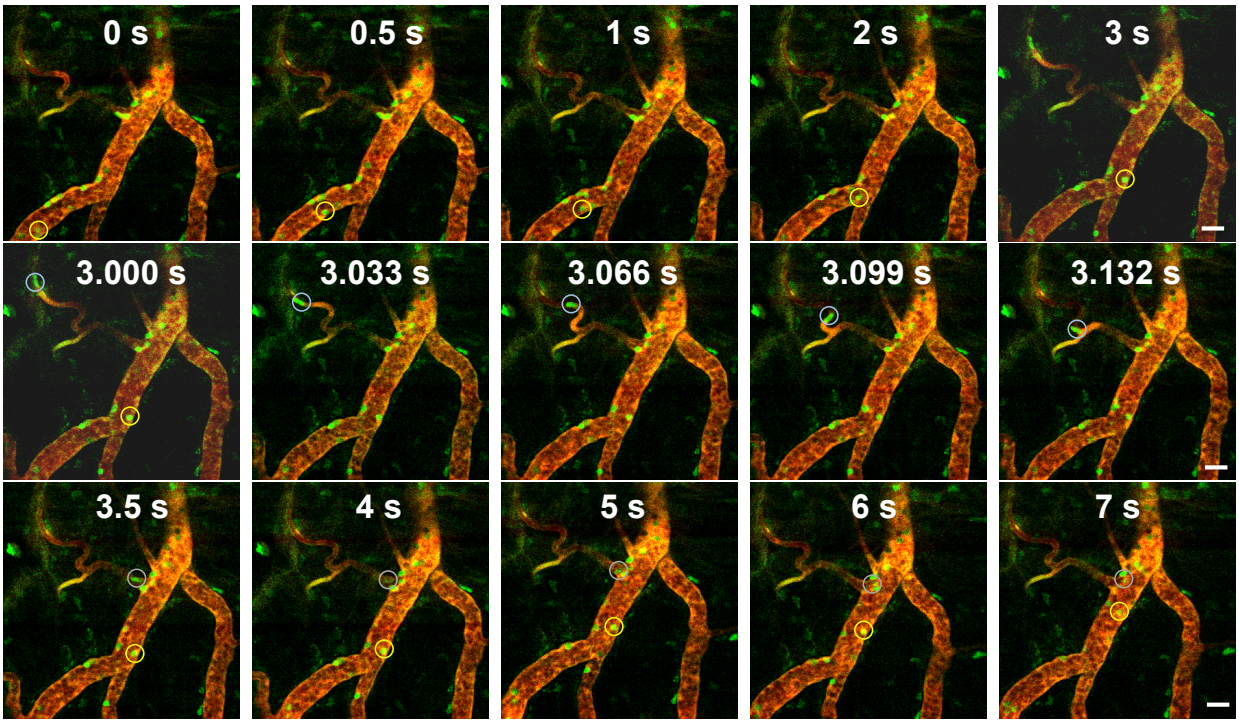

Figure S5. ***In vivo*** **real-time monitoring of CX3CR1^{+} Ly6C^{low} monocytes in CRCs during anti-VEGFR2 therapy.** Snapshot images of Movie S1 showing various behaviors of CX3CR1^{+} Ly6C^{low} monocytes inside the blood vessels. Grey, flowing. Yellow, rolling. Scale bar, 50 μm.

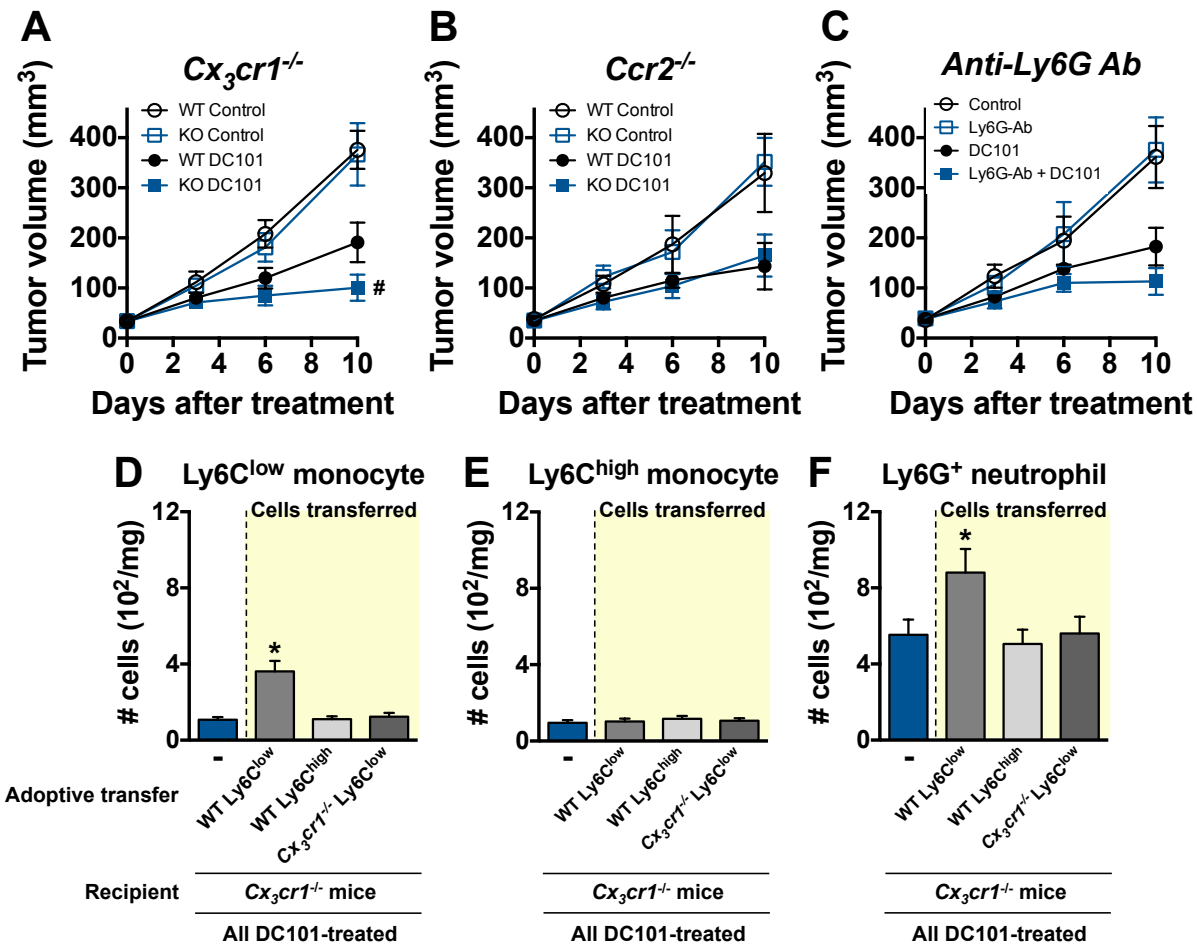

Figure S6. Blockade of CX3CR1-dependent infiltration of Ly6C^{low} monocytes improves efficacy of anti-VEGFR2 therapy. (**A** to **C**) SL4 tumor growth. Tumor volume was measured using a high-frequency ultrasound imaging system for C57BL/6 mice bearing orthotopically grown syngeneic SL4 tumors. (**A**) The effect of CX3CR1 deletion on SL4 tumor growth. SL4 tumors were grown in C57BL/6 WT mice or *Cx$_3$cr1$^{-/-}$* (CX3CR1 KO) mice and treated with either control rat IgG or DC101. Data are represented as mean ± SEM. n=8/group. ANOVA with Holm-Sidak post-hoc test. #, $p < 0.05$ versus WT DC101. (**B**) The effect of CCR2 deletion on SL4 tumor growth. SL4 tumors were grown in C57BL/6 WT mice or *Ccr2$^{-/-}$* (CCR2 KO) mice and treated as indicated. Data are represented as mean ± SEM. n=8/group. (**C**) The effect of administration of anti-Ly6G antibody on SL4 tumor growth. SL4 tumor-bearing C57BL/6 WT mice were treated with either control rat IgG, anti-Ly6G antibody, DC101, or anti-Ly6G antibody + DC101. Data are represented as mean ± SEM. n = 8 / group. Data are representative of three independent experiments. (**D** to **F**) Monocytes and neutrophils in SL4 tumors (**Figure 5D**).

DC101-treated *Cx$_3$cr1$^{-/-}$* mice received adoptive transfer of either tumor-isolated WT Ly6C^{low} monocytes (Ly6C^{low}), WT Ly6C^{high} monocytes (Ly6C^{high}), or Ly6C^{low} monocytes isolated from tumors of *Cx$_3$cr1$^{-/-}$* mice (KO Ly6C^{low}). Each subset of myeloid cells in tumor infiltrate was analyzed on day 12 by flow cytometry. Data are represented as mean ± SEM. ANOVA with Holm-Sidak post-hoc test. n = 8 / group. *, $p < 0.05$ versus *Cx$_3$cr1$^{-/-}$* control mice without cell transfer (blue bar). The graphs depict data for the absolute number of cells per mg of tumor tissue.

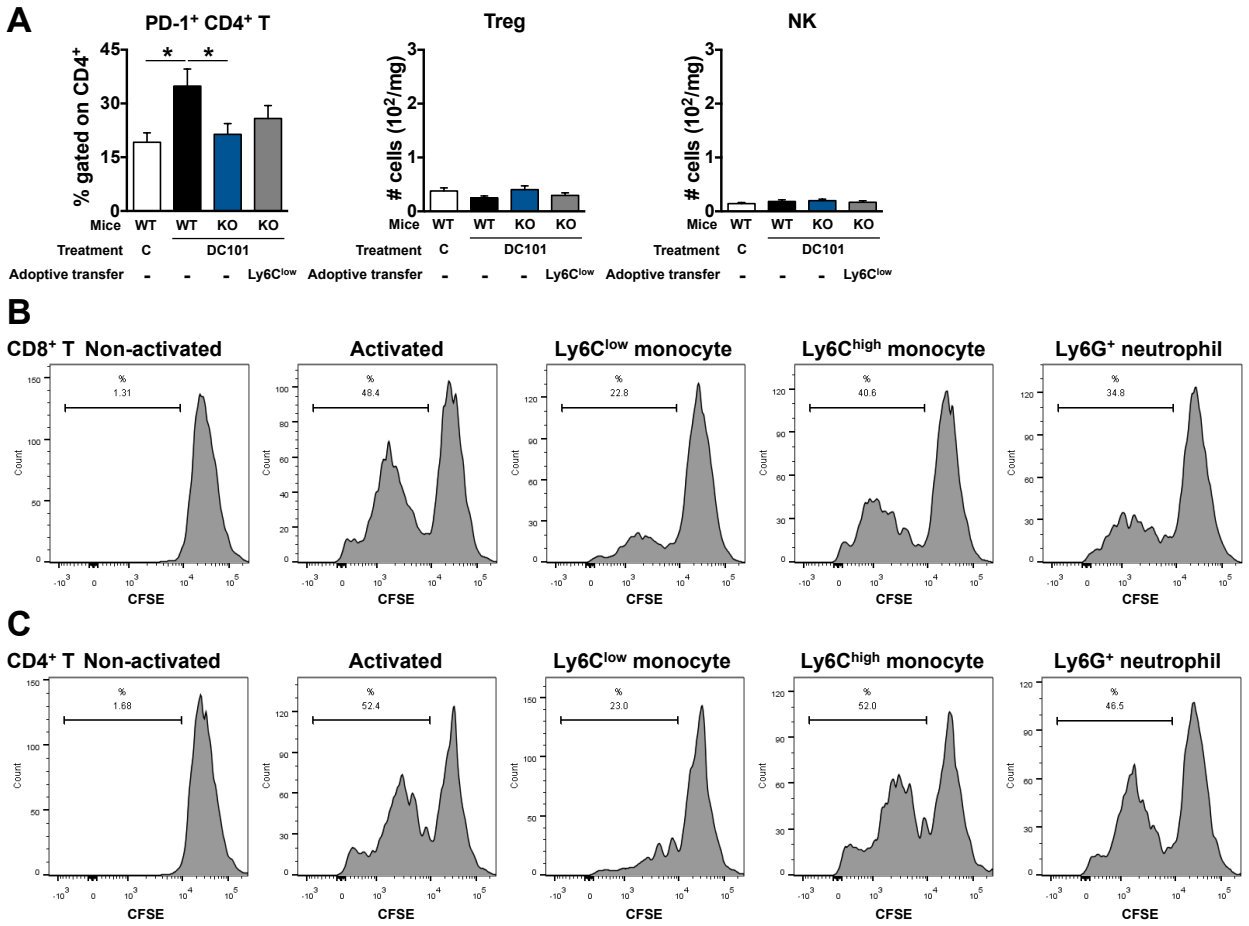

Figure S7. Ly6C^{low} monocytes drive immunosuppression during anti-VEGFR2 treatment in CRCs.

(**A**) Flow cytometric analysis of PD-1$^+$ CD4$^+$ T cells, regulatory T cells (Treg), and NK cells in SL4 tumors as indicated. *White bar*, WT mice bearing SL4 tumors treated with control rat IgG; *Black bar*, WT mice bearing SL4 tumors treated with DC101; *Blue bar*, *Cx$_3$cr1$^{-/-}$* mice bearing SL4 tumors treated with DC101 without cell transfer; *Grey bar*, DC101-treated *Cx$_3$cr1$^{-/-}$* mice received adoptive transfer of tumor-isolated WT Ly6C^{low} monocytes. The PD-1$^+$ CD4$^+$ T graphs depict data for PD-1$^+$ populations relative to total CD4$^+$ T cells. The Treg and NK graphs depict data for the absolute number of cells per mg of tumor tissue. The lymphocyte infiltrate in the tumor was analyzed on day 12 by flow cytometry. Data are represented as mean ± SEM. n = 8 / group. ANOVA with Holm-Sidak post-hoc test. *, $p < 0.05$. (**B**) Representative flow cytometric analyses of nonactivated or activated CD8$^+$ T cell proliferation. CellTrace-labeled splenic CD8$^+$ T cells from syngeneic mice were activated and cocultured with either tumor-isolated Ly6C^{low} monocytes, Ly6C^{high} monocytes, or Ly6G$^+$ neutrophils. Data are representative of three independent experiments. (**C**) Representative flow cytometric analyses of nonactivated or

activated $CD4^+$ T cell proliferation. CellTrace-labeled splenic $CD4^+$ T cells from syngeneic mice were activated and co-cultured with either tumor-isolated $Ly6C^{low}$ monocytes, $Ly6C^{high}$ monocytes, or $Ly6G^+$ neutrophils. All data are representative of three independent experiments.

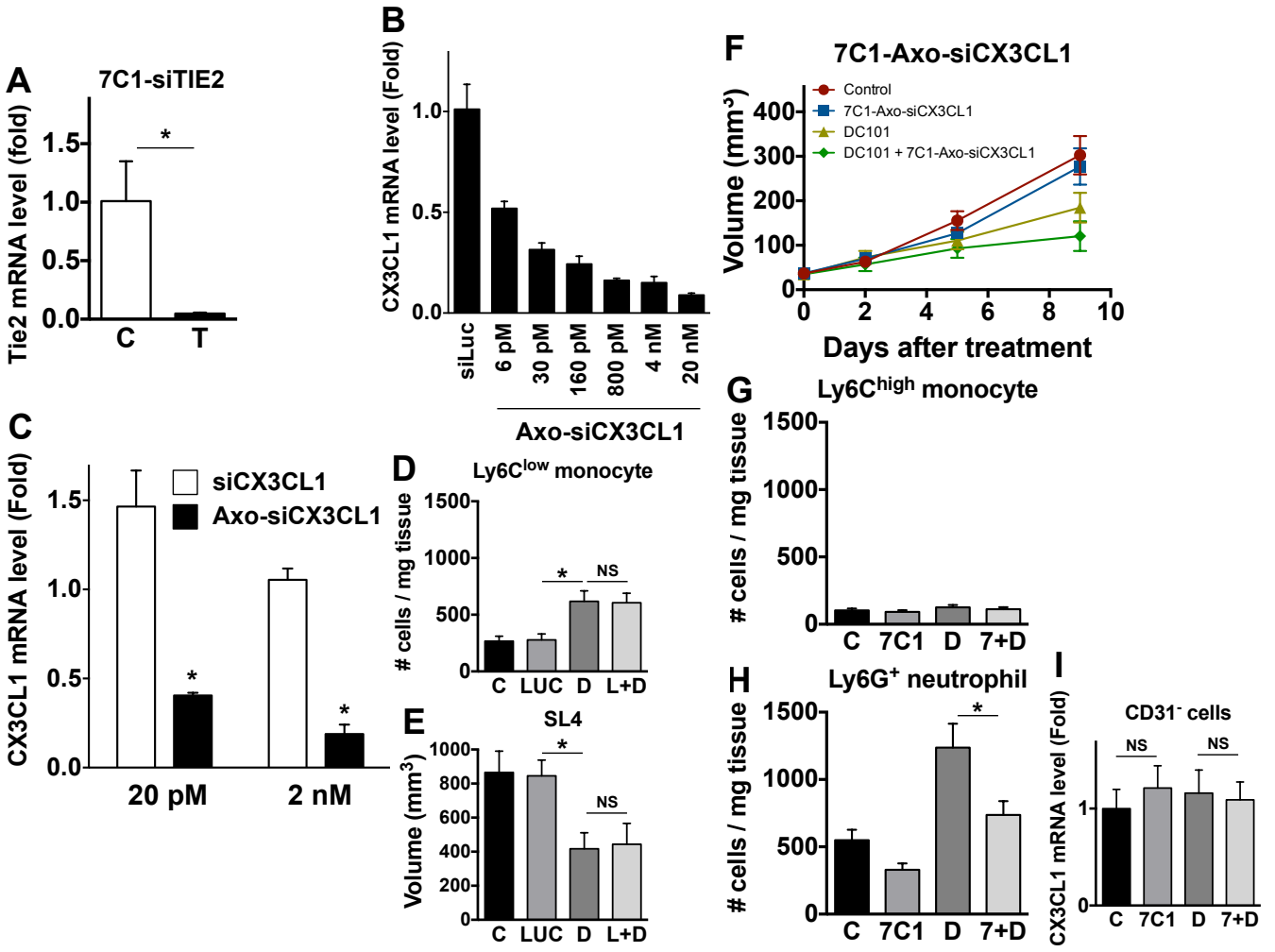

Figure S8. ***In vivo*** **nanoparticle delivery of siCX3CL1 inhibits Ly6C^{low} monocyte infiltration and enhances efficacy of anti-VEGFR2 therapy.** (**A**) C57BL/6 WT mice bearing orthotopically grown syngeneic SL4 CRCs were treated with either control vehicle or 7C1-siTie2. Relative Tie2 mRNA expression levels in endothelial cells isolated from SL4 tumors were determined on day 2 after treatment by quantitative real-time PCR, normalized against GAPDH. Data are represented as mean ± SEM. n = 5 / group. Two-tailed t test. *, $p < 0.05$. (**B**) The dose-response curve for the duplex that performed best in the *In vitro* screening of siCX3CL1 candidate duplexes which was selected for *in vivo* use (Axo-siCX3CL1, indicated by red box in **Figure 7B**). Relative CX3CL1 mRNA expression level in endothelial cells *in vitro* normalized to siLUC (Luciferase) control. Data are represented as mean ± SEM. Data are representative of three independent experiments. (**C**) Comparison of the knock-down efficiency of our Axo-siCX3CL1 and another siRNA against CX3CL1 (siCX3CL1) from a recent publication (Morari et al., 2014). Data are represented as mean ± SEM. Each siRNA was transfected

twice and mRNA analysis was run in triplicates. Two-tailed t test. *, $p < 0.05$ versus siCX3CL1. (**D**) Ly6C^{low} monocytes in SL4 tumors treated with either control rat IgG (C), 7C1-siLUC (LUC), DC101 (D), or 7C1-siLUC + DC101 (L+D). Ly6C^{low} monocytes in tumor infiltrate were analyzed on day 12 after treatment by flow cytometry Data are represented as mean ± SEM. n = 5 / group. ANOVA with Holm-Sidak post-hoc test. *, $p < 0.05$. NS, non-significant. (**E**) Tumor volume of SL4 measured on day 12 after treatment as indicated. n = 5 / group. Data are represented as mean ± SEM. ANOVA with Holm-Sidak post-hoc test. *, $p < 0.05$. NS, non-significant. (**F**) SL4 tumor growth. Tumor volume was measured using a high-frequency ultrasound imaging system for C57BL/6 mice bearing orthotopically grown syngeneic SL4 tumors treated as indicated. Data are represented as mean ± SEM. n = 8 / group. (**G** and **H**) Ly6C^{high} monocytes (**G**) and Ly6G^{+} neutrophils (**H**) in SL4 tumors treated with either control rat IgG (C), 7C1-Axo-siCX3CL1 (7C1), DC101 (D), or 7C1-Axo-siCX3CL1 + DC101 (7+D). Ly6C^{high} monocytes and Ly6G^{+} neutrophils in tumor infiltrate were analyzed on day 12 after treatment by flow cytometry. Data are represented as mean ± SEM. n = 8 / group. ANOVA with Holm-Sidak post-hoc test. *, $p < 0.05$. The graphs depict data for the absolute number of cells per mg of tumor tissue. (**I**) Relative CX3CL1 mRNA expression levels in non-endothelial cells from SL4 tumors were determined on day 12 after treatment by quantitative real-time PCR, normalized against GAPDH. n = 8 / group. Data are represented as mean ± SEM. ANOVA with Holm-Sidak post-hoc test. NS, non-significant.

Supplemental Movies

Movie S1. *In vivo* real-time monitoring of CX3CR1^{+} Ly6C^{low} monocytes in CRCs during anti-VEGFR2 therapy. Movie of EGFP^{+} CX3CR1^{+} Ly6C^{low} monocytes (green) and blood vessels (red) in CRC of a *Cx3cr1$^{gfp/+}$* mouse bearing SL4 tumor at 6 days after DC101 treatment.

Note: The original raw movie with 512 by 512 pixels per frame was compressed (H.264) and resized to 256 x 256 pixels per frame to reduce the file size.

Movie S2. Ly6C^{low} monocytes require CX3CR1 to infiltrate into tumors. Movie of wild-type Ly6C^{low} monocytes (green) and blood vessels (red) in CRC of a wild-type mouse bearing SL4 tumor at 5 days after DC101 treatment. Ly6C^{low} monocytes were isolated from DC101-treated SL4 tumor-bearing C57BL/6 wild-type mice (WT), fluorescently labeled, and adoptively transferred into DC101-treated SL4 tumor-bearing C57BL/6 WT animals.

Note: The original raw movie with 512 by 512 pixels per frame was compressed (H.264) and resized to 256 x 256 pixels per frame to reduce the file size.

Movie S3. Ly6C^{low} monocytes require CX3CR1 to infiltrate into tumors. Movie of CX3CR1-deficient Ly6C^{low} monocytes (green) and blood vessels (red) in CRC of a wild-type mouse bearing SL4 tumor at 5 days after DC101 treatment. Ly6C^{low} monocytes were isolated from DC101-treated SL4 tumor-bearing C57BL/6 *Cx3cr1$^{-/-}$* mice (KO), fluorescently labeled, and adoptively transferred into DC101-treated SL4 tumor-bearing C57BL/6 WT animals.

Note: The original raw movie with 512 by 512 pixels per frame was compressed (H.264) and resized to 256 x 256 pixels per frame to reduce the file size.